

# Floquet topological phase transitions in a kicked Haldane-Chern insulator

Tridev Mishra,<sup>1,\*</sup> Anurag Pallaprolu,<sup>1,†</sup> Tapomoy Guha Sarkar,<sup>1,‡</sup> and Jayendra N. Bandyopadhyay<sup>1,§</sup>

<sup>1</sup>*Department of Physics, Birla Institute of Technology and Science, Pilani 333031, India.*

We consider a periodically  $\delta$ -kicked Haldane type Chern insulator with the kicking applied in the  $\hat{z}$  direction. This is known to behave as an inversion symmetry breaking perturbation, since it introduces a time-dependent staggered sub-lattice potential. We study here the effects of such driving on the topological phase diagram of the original Haldane model of a Hall effect in the absence of a net magnetic field. The resultant Floquet band topology is again that of a Chern insulator with the driving parameters, frequency and amplitude, influencing the inversion breaking mass  $M$  of the undriven Haldane model. A family of such, periodically related, ‘Semenoff masses’ is observed to occur which support a periodic repetition of Haldane like phase diagrams along the inversion breaking axis of the phase plots. Out of these it is possible to identify two in-equivalent masses in the reduced zone scheme of the Floquet quasienergies, which form the centres of two inequivalent phase diagrams. Further, variation in the driving amplitude’s magnitude alone is shown to effect the topological properties by linearly shifting the phase diagram of the driven model about the position of the undriven case. A phenomenon that allows the study of Floquet topological phase transitions in the system. Finally, we also discuss some issues regarding the modifications to Haldane’s condition for preventing band overlaps at the Dirac point touchings in the Brillouin zone, in the presence of kicking.

## I. INTRODUCTION

Topology and notions intrinsic to it were introduced into the band theory of solids through the work of Thouless, Halperin and others [1–5] while theoretically exploring the remarkable phenomenon of the Integer Quantum Hall Effect (IQHE) [6, 7]. Many such exotic features were predicted and identified for other associated phenomena, which went beyond conventional time-reversal symmetry breaking, such as the Quantum Spin Hall Effect (QSHE), in graphene and other topological materials [8–11]. Experimentally, this has sparked off a flurry of activity directed towards the synthesis of materials and nano structures which exhibit such novel features [12–17]. As such shaping the field of ‘Topological Insulators’. From a theoretical perspective, the broad objective has been to achieve a comprehensive classification scheme for these insulators [18–20].

Graphene, beyond its much touted mechanical and transport properties [21–23], has shown itself to be rich in topological features [24, 25] and various topological aspects of the honeycomb lattice have been investigated in cold-atom and photonic-crystal setups [26–30]. Studies of graphene irradiated or periodically driven by circularly polarized light have revealed rich topological textures beyond those seen in the undriven case [31–40]. An entire sub-domain of “Floquet Topological Insulators” [41] has emerged as a result, which constitutes those systems that exhibit topological ground states and edge phenomena in the presence of certain time-dependent periodic potentials [42]. They have offered unprecedented control

and freedom to engineer new topological phases and edge state (in some cases Majorana modes) behaviors [43–62] as well as a knob to study topological phase transitions in cold-atom or photonic crystal setups [63–69]. The theoretical classification of Floquet topological insulators and the identification of valid topological invariants that correctly characterize the bulk-edge correspondence for these systems is an on-going effort [70–77].

Of late, the use of delta-function kicks has also been shown to impart interesting topological properties in the form of new Floquet topological phases such as semi-metallic phases in Harper models [78], chiral edge modes in Quantum Hall systems [79], appearance of unexpected topological equivalence between spectrally distinct Hamiltonians [80] as well as generation of Majorana end modes in 1-D systems [81]. This has led to interest in studying Dirac systems especially graphene, its nano-ribbons and other hexagonal lattice models such as the Kitaev model under periodic driving or kicking [82–84]. In fact a very recent work has studied the effects of periodic kicking on the topological properties of the Qi-Wu-Zhang (QWZ) Chern insulator [85] and shown the emergence of higher Chern number phases in certain cases. In this work we shall be considering a form of kicking which is found to introduce a Semenoff like mass, hence no topological nontrivialities (in the absence of time reversal symmetry breaking) in the spectrum of planar Graphene but, shows some promise as far as manipulating the topology of Haldane-like Chern insulators is concerned.

The recent success in realizing the Haldane model experimentally [30] within the framework of ultracold atoms in optical lattices has opened a doorway to engineering various kinds of Chern insulators, using the paradigm of shaken optical lattices and the Floquet formalism, and studying topological transitions in them [67, 69, 86]. These realizations offer an appreciable degree of tunability and provide an encouraging platform

\* tridev.mishra@pilani.bits-pilani.ac.in

† anurag.pallaprolu@gmail.com

‡ tapomoy1@gmail.com

§ jnbandyo@gmail.com

for the study of Haldane systems under periodic driving. We consider these setups as possible avenues for realizing the kind of delta-kicked Haldane model which is the centerpiece of our study. Beyond the cold atom setups, an interesting recent experiment [40] drives graphene itself using ultra-fast, short-duration low frequency laser pulses of circularly polarized light which open local gaps in the Floquet quasi-energies of the irradiated graphene. This procedure hints at the creation of local Haldane like band structures but their topological classification has issues that need to be addressed. A more viable candidate for an actual material realization of the Haldane model is presented in [87] where, a honeycomb lattice, specifically Silicene, with out-of-plane staggering of sublattice sites, effectively realizes Haldane's prescription of a staggered magnetic field upon being subjected to an in-plane magnetic field which could be made very weak. Other interesting proposals exist, that realize Chern insulators either using electron correlations at low dimensions, in say double perovskite hetero-structures [88], or the notion of in-plane magnetic fields, such as in perovskite monolayers [89] and laterally patterned  $p$ -type semiconductor hetero-structures with low-symmetry interfaces [90]. The proposal in [87], along with the suggestions in [84] that outline methods to implement a kicking using hexagonal boron nitride over graphene [91–93], provide the broad experimental context in which our system has some hope of being realized. This motivates our academic interest in the study undertaken here.

In this paper, we begin with an overview of various features of the Haldane model, broadly describing its spectral and topological aspects in Sec.II. This is followed by the description and analysis of our choice of a kicked Haldane model in Sec.II B and a brief introduction to the computation of the Chern topological invariant in Sec.III. A detailed exposition of the various properties and behavior of the kicked model is provided in the Sec.IV, on results and discussion, and Sec.V deals with certain possible experimental realizations and heating issues related to our model. We see that, the kicking scheme incorporates itself into the effective Hamiltonian in a way that it provides a means of manipulating the inversion symmetry breaking parameter of the Haldane model which is essentially the staggered off-set to the on-site energies at the two closest neighboring sites of the two interpenetrating triangular sub-lattices  $A$  and  $B$ . This and various other aspects are discussed therein, followed by a conclusion comparing our work to related studies.

The kicking protocol studied in this paper has the effect of breaking inversion symmetry and opening a gap in graphene. This, however, does not lead to the appearance of any non-trivial topological features in graphene as the equal gap/mass term at the two Dirac points is of the Semenoff kind. We observe that in our present problem the general effect of the driving is to modify the inversion breaking energy of the Haldane model.

## II. THE KICKED HALDANE MODEL

### A. The Undriven Haldane Model

The Haldane model [94] is a perfectly 2-dimensional Quantum Hall insulator with the unique property of exhibiting Quantum Hall behavior in the absence of any net magnetic field through any of its unit cells. It consists of a 2-D hexagonal lattice of atoms, with a single tight binding orbital at each of the two lattice sites within a unit cell. These are the two distinct sites belonging to the  $A$  and  $B$  triangular sub-lattices as shown in Fig. (1) by filled and hollow points respectively. Normally, such a lattice shows a semimetallic band structure which is well known from Graphene. However, to realize an insulator, the degeneracies at the Dirac points in the 2-D Brillouin zone need to be lifted by breaking the inversion and time-reversal symmetries in the system. In the Haldane model these are broken to ensure Quantum Hall behavior. The inversion symmetry is broken by giving an off-set to the on-site energies at the two inequivalent nearest neighbor sites  $A$  and  $B$  by an amount  $-M$  and  $+M$  respectively. Breaking inversion symmetry opens a gap at the band touchings in the Brillouin zone and makes the system a semiconductor/normal insulator. In order to get a topological insulator it is further required to break time-reversal symmetry which is done here by making the hoppings to the next to nearest-neighbor sites complex valued as,  $t_2 e^{\pm i\phi}$ ,  $t_2$  being real. The nearest neighbor hoppings  $t_1$  on the other hand remain real valued. An ingenious choice of magnetic field helps to ensure this by making the overall magnetic flux through any of the hexagons (unit cells) of the lattice zero and

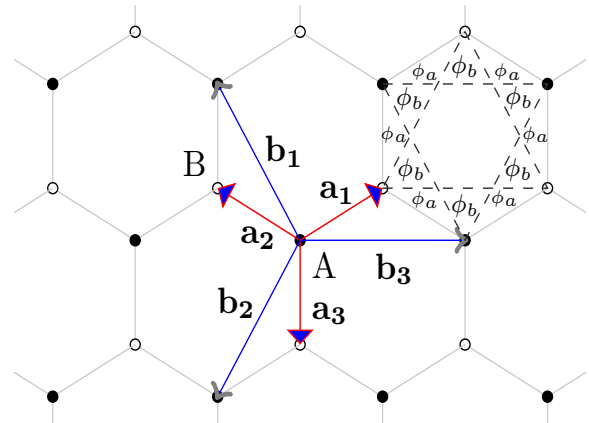


FIG. 1. Schematic illustrating the honeycomb lattice with vectors to the nearest and next nearest neighbors of an  $A$  sublattice site. A flux configuration, where  $\phi_a$  and  $\phi_b$  are fluxes through the triangles that bound each of the labeled regions, is also shown which can make the next to nearest neighbor hoppings phase dependent with zero net flux in the hexagon i.e.  $(\phi_a + \phi_b) = 0$ .

hence realizes a globally vanishing magnetic field while at the same time breaking time-reversal symmetry. Though this does require the local existence of a spatially periodic magnetic field everywhere, perpendicularly applied to the lattice plane. It gives rise to a flux arrangement that collectively disappears over a unit cell. One such choice is illustrated in Fig. (1), where the condition  $(\phi_a + \phi_b) = 0$  fulfills this requirement. Several such choices are permitted by gauge freedom and since travelling along the sides of any hexagon encloses zero flux the  $t_1$  hoppings acquire no phase contribution. The hopping term  $t_2$  for the next to nearest neighbor sites acquires phases in hops around triangular cells which enclose non-zero flux. For the case in Fig. (1) this phase  $\phi$  comes out to be  $2\pi(2\phi_a + \phi_b)/\phi_0$  expressed in units of the flux quantum  $\phi_0$ .

The need to break time-reversal invariance arises from the familiar requirement encountered in the IQHE [1, 2, 6, 7] that for non-zero quantized transverse conductance  $\sigma_{xy}$ , time-reversal invariance must be absent in the system as otherwise  $\sigma_{xy}$  is an odd function and amounts to zero. It is the behavior of the gap that opens at the Dirac points also called the mass term from the low energy, (2+1)-D relativistic linearization approximation, that crucially determines the existence of the Hall conductance. In the presence of just broken inversion symmetry this mass term ( $M$ ) is a Semenoff mass which has the same sign at both Dirac points and yields  $\sigma_{xy} = 0$  which follows from the definition for the Chern invariant, in this case. However if time reversal invariance is

absent the mass term ( $\phi$  dependent) has opposite signs at these points and leads to a non-zero  $\sigma_{xy}$ . When both parameters  $M$  and  $\phi$  are zero the bands touch at points in the Brillouin zone called Dirac points owing to the linear dispersion in the vicinity of these degeneracies. These are high symmetry points in the Brillouin zone in addition to the band center. In this situation the system is semi-metallic and allows a two-dimensional representation at these high symmetry points. When the symmetry breaking parameters take on other combinations of values the system is found to belong to insulating regions with the Chern number  $\mathcal{C}$ , for the valence band (lower band with the Fermi energy in the gap at zero temperature) taking values  $\pm 1, 0$  depending on the relative strengths of the two parameters. These regions of different conductance values  $\sigma_{xy} = \mathcal{C}e^2/h$  are separated by a boundary where the gap closes at either one of the Dirac points in the Brillouin zone. These touchings are the transition band configurations where  $\mathcal{C}$ 's for the two bands can rearrange themselves by assuming values that add up to zero thereby ensuring the standard requirement that the total band bundle remains topologically trivial [3]. These and other properties of the model follow from its Hamiltonian and the linear approximation to it at the band touchings. We now take a closer look at this Hamiltonian which will serve as the target system for the intended driving scheme.

The two dimensional Haldane Hamiltonian in reciprocal space, as obtained from its real space tight binding form is

$$H(\mathbf{k}) = 2It_2 \cos \phi \sum_i \cos(\mathbf{b}_i \cdot \mathbf{k}) + t_1 \left[ \sum_i \{ \sigma^x \cos(\mathbf{a}_i \cdot \mathbf{k}) + \sigma^y \sin(\mathbf{a}_i \cdot \mathbf{k}) \} \right] + \sigma^z \left[ M - 2t_2 \sin(\phi) \sum_i \sin(\mathbf{b}_i \cdot \mathbf{k}) \right] \quad (1)$$

Here, the quasi-momentum  $\mathbf{k}$  is a good quantum number since the choice of magnetic field preserves the original translation symmetry of the lattice,  $\mathbf{I}$  is the  $2 \times 2$  identity element and  $\sigma^x, \sigma^y$  and  $\sigma^z$  are the Pauli matrices. From Fig.(1) the vectors  $\mathbf{a}_1 \equiv \left( \frac{\sqrt{3}a}{2}, \frac{a}{2} \right)$ ,  $\mathbf{a}_2 \equiv \left( -\frac{\sqrt{3}a}{2}, \frac{a}{2} \right)$  and  $\mathbf{a}_3 \equiv (0, -1)$  are the vectors from an  $A$  sub-lattice site to the nearest neighboring  $B$  sub-lattice sites. The  $a$  stands for the length of the bond joining nearby  $A$  and  $B$  sites. This choice is a matter of convention here and is defined by these vectors forming a closed right handed system with the cross product of any two in increasing sequence of the indices being aligned out of the plane in the direction of positive  $\hat{z}$ . While, as seen in the same figure, the

vectors to the next nearest neighbor sites are chosen as  $\mathbf{b}_1 = \mathbf{a}_2 - \mathbf{a}_3$ ,  $\mathbf{b}_2 = \mathbf{a}_3 - \mathbf{a}_1$  and  $\mathbf{b}_3 = \mathbf{a}_1 - \mathbf{a}_2$ . Thus the summation index in the above Hamiltonian extends over these three possibilities for both kinds of vectors. The reciprocal space lattice for this system is also hexagonal and therefore first Brillouin zone (FBZ) is a hexagon with band touchings occurring at the zone corners. The FBZ comprises of two in-equivalent band touchings or Dirac points  $\mathbf{K}$  and  $\mathbf{K}'$ . It is possible to rearrange this hexagonal FBZ into an equivalent rhomboidal one by shifting regions of the former by reciprocal lattice vectors. Within this description the Dirac points lie inside the FBZ and are given by  $\mathbf{K} = \left( \frac{2\pi}{3\sqrt{3}a}, \frac{2\pi}{3a} \right)$  and  $\mathbf{K}' = \left( \frac{4\pi}{3\sqrt{3}a}, 0 \right)$ . The two band energy dispersion that follows from the above Hamiltonian is

$$E_{\pm}^H(\mathbf{k}) = 2t_2 \cos(\phi) \left[ 2 \cos\left(\frac{3ak_y}{2}\right) \cos\left(\frac{\sqrt{3}ak_x}{2}\right) + \cos(\sqrt{3}ak_x) \right] \pm \left\{ t_1^2 \left[ 2 \cos\left(\frac{ak_y}{2}\right) \cos\left(\frac{\sqrt{3}ak_x}{2}\right) + \cos(k_y) \right]^2 + t_1^2 \left[ 2 \sin\left(\frac{ak_y}{2}\right) \cos\left(\frac{\sqrt{3}ak_x}{2}\right) - \sin(k_y) \right]^2 + \left[ M - 2t_2 \sin(\phi) \times \left( -2 \cos\left(\frac{3ak_y}{2}\right) \sin\left(\frac{\sqrt{3}ak_x}{2}\right) + \sin(\sqrt{3}ak_x) \right) \right]^2 \right\}^{\frac{1}{2}} \quad (2)$$

On substituting the coordinates for either of the Dirac points  $\mathbf{K}$  or  $\mathbf{K}'$  in the above expression one gets  $M - 3\sqrt{3}t_2 \sin(\phi)$  and  $M + 3\sqrt{3}t_2 \sin(\phi)$  respectively. From this we arrive at the condition for the bands to touch at these points as  $M = 3\sqrt{3}\nu t_2 \sin(\phi)$  where  $\nu = \pm 1$  depending on the particular Dirac point under consideration. Touching at both points occurs only when both inversion and time-reversal are present i.e both  $M$  and  $t_2 \sin(\phi)$  are zero. The touchings at individual Dirac points occur in Haldane's Chern number phase diagram at the transition boundaries where  $\mathcal{C}$  undergoes a discrete step in its value.

An important aspect of the model is the constraint on the relative strengths of the hopping parameters given by  $|t_2/t_1| < 1/3$  that ensures that the bands of the model do not overlap. This is useful for a clear observation of the band touchings in any physical realization of the model as it ensures that the upper and lower bands are always well separated by a gap unless they touch with the energies at these touchings being extremal points or maximas if one considers the lower band. We will discuss this condition in the context of kicking later on to see how it gets modified for the kicked system and also ascertain how it may be used to define a magnitude scale for the strength of the driving. Now, we move on to the model of interest in the present work which is the Haldane Hamiltonian under kicking.

## B. Driven Haldane Model

The choice of driving the Haldane model using a periodic train of delta function kicks allows an exact Floquet treatment of the stroboscopic kind without recourse to a high frequency approximation of the kind used in [55, 95]. Central to such approaches, and the marked rise of interest in Floquet topological insulators, is the possibility of having a controllable parameter whose variation helps to tune the system from a normal to a topological insulator, or through different topological phases. Thus a system may be designed where, by sweeping an experimentally controllable parameter across a prescribed range of values, one could transition the total Chern number of the filled bands of the system between trivial and non-trivial values. Much like the different quantized conductance values assumed by the system in the IQHE when the magnetic field is swept adiabatically. The added advantage driving has to offer here, is that it achieves all

this in relatively simpler, non-interacting effective static Hamiltonians. Since, in general, topological characteristics are robust features of a system and are unaffected by perturbations to a large extent, having systems which do show transitions from normal to topological insulators (and vice-versa) in a discrete manner is of considerable interest. This is so because interesting properties of the valence band Bloch functions are known to occur at the transitions such as, lack of a maximally localized Wannier representation in the Chern insulating phase and anomalous localization behavior of the wavefunctions [96, 97]. Thus the transitions merit some attention in various systems where they can be realized in a manner which permits a simpler analytical/numerical approach to their study. Our kicked model belongs to this category of systems.

Prior to expressing the Hamiltonian in the presence of kicking it would be useful to adopt some notation to denote terms in Eqs. (1) and (2). The structure of the Hamiltonian in Eq.(1) is of the general form  $H(\mathbf{k}) = h_0(\mathbf{k})\mathbf{I} + \mathbf{h}(\mathbf{k}) \cdot \boldsymbol{\sigma}$ , where  $\boldsymbol{\sigma} = (\sigma^x, \sigma^y, \sigma^z)$  is the vector of Pauli matrices and

$$h_0(\mathbf{k}) = 2t_2 \cos(\phi) \left[ 2 \cos\left(\frac{3ak_y}{2}\right) \cos\left(\frac{\sqrt{3}ak_x}{2}\right) + \cos(\sqrt{3}ak_x) \right].$$

The  $\mathbf{h}(\mathbf{k})$  here, is the vector  $[t_1 L(\mathbf{k}), t_1 F(\mathbf{k}), M - 2t_2 \sin(\phi)N(\mathbf{k})]$  with

$$L(\mathbf{k}) = 2 \cos\left(\frac{ak_y}{2}\right) \cos\left(\frac{\sqrt{3}ak_x}{2}\right) + \cos(k_y)$$

$$F(\mathbf{k}) = 2 \sin\left(\frac{ak_y}{2}\right) \cos\left(\frac{\sqrt{3}ak_x}{2}\right) - \sin(k_y)$$

$$N(\mathbf{k}) = -2 \cos\left(\frac{3ak_y}{2}\right) \sin\left(\frac{\sqrt{3}ak_x}{2}\right) + \sin(\sqrt{3}ak_x)$$

It follows that

$$|\mathbf{h}(\mathbf{k})| = \sqrt{t_1^2 L^2(\mathbf{k}) + t_1^2 F^2(\mathbf{k}) + (M - 2t_2 \sin(\phi)N(\mathbf{k}))^2}.$$

The driving scheme is chosen to be a train of delta function kicks which are separated by fixed time interval  $T$ . Such a scheme was introduced in the context of driving a hexagonal lattice, in particular graphene, as a platform for synthesizing novel dispersion relations and wave packet dynamics [84]. This work proposes using a kicking

which is applied as the following perturbing term to the Hamiltonian

$$\mathcal{H}_{kick,\mathbf{k}}(t) = (\alpha_x \sigma^x + \alpha_y \sigma^y + \alpha_z \sigma^z) \sum_{m=-\infty}^{m=\infty} \delta(t-mT) \quad (3)$$

and represents a general  $2 \times 2$  kicking protocol with the  $SU(2)$  pseudo-spin structure of the 2-dimensional Haldane Hamiltonian. The  $\alpha_x$ ,  $\alpha_y$  and  $\alpha_z$  stand for kicking amplitudes in the respective directions. Since we are consistently expressing the Hamiltonian and the perturbation to it in  $\mathbf{k}$ -space, the kicking is applied uniformly to every unit cell of the lattice to have the reciprocal space representation of the above form. The dynamics of the system over a period  $T$ , under such a perturbation, are governed by an evolution operator  $U_{XYZ} = U_{kick}U_{static} = e^{-i\boldsymbol{\alpha}\cdot\boldsymbol{\sigma}}e^{-i\mathcal{H}(\mathbf{k})T}$  where,  $U_{XYZ} =$

$e^{-i\mathcal{H}_{XYZ}(\mathbf{k})T}$  with  $\mathcal{H}_{XYZ}(\mathbf{k})$  as the Floquet Hamiltonian and,  $\boldsymbol{\alpha}$  and  $\boldsymbol{\sigma}$  are  $(\alpha_x, \alpha_y, \alpha_z)$  and  $(\sigma^x, \sigma^y, \sigma^z)$  respectively. Using the algebra of Pauli matrices and some standard results associated with them, it is possible (as illustrated in [84]) to obtain the exact form of  $\mathcal{H}_{XYZ}(\mathbf{k})$ , see appendix. In particular, we are interested in a kicking scheme where  $\alpha_z \neq 0$  while  $\alpha_x = \alpha_y = 0$  and henceforth assume these parameter values in the perturbing Hamiltonian in eq.(3). Thus we are interested in the  $\hat{z}$ -kicked Haldane model whose Hamiltonian we denote  $\mathcal{H}_Z(\mathbf{k})$  which is obtained from  $\mathcal{H}_{XYZ}(\mathbf{k})$  by putting in the requisite conditions. The calculation of  $\mathcal{H}_{XYZ}(\mathbf{k})$  in the manner outlined in [84] will involve considering only the vector  $\mathbf{h}(\mathbf{k})$  projected along the Pauli matrices. The diagonal part due to  $h_0$  remains unmodified and finally shows up in the expression for  $\mathcal{H}_Z(\mathbf{k})$  which is again of the structure  $h_0(\mathbf{k})\mathbf{I} + \epsilon_z(\mathbf{k})\mathbf{h}'(\mathbf{k}) \cdot \boldsymbol{\sigma}$ . The vector  $\mathbf{h}'(\mathbf{k})$  is represented by components  $(h'_x(\mathbf{k}), h'_y(\mathbf{k}), h'_z(\mathbf{k}))$  which are

$$\begin{aligned} h'_x(\mathbf{k}) &= \frac{1}{\sin(T\epsilon_z)} \left[ \frac{-t_1 L(\mathbf{k})}{|\mathbf{h}(\mathbf{k})|} \sin(T|\mathbf{h}(\mathbf{k})|) \cos(\alpha_z) + \text{sgn}(\alpha_z) \frac{t_1 F(\mathbf{k})}{|\mathbf{h}(\mathbf{k})|} \sin(\alpha_z) \sin(T|\mathbf{h}(\mathbf{k})|) \right] \\ h'_y(\mathbf{k}) &= \frac{1}{\sin(T\epsilon_z)} \left[ \frac{-t_1 F(\mathbf{k})}{|\mathbf{h}(\mathbf{k})|} \sin(T|\mathbf{h}(\mathbf{k})|) \cos(\alpha_z) - \text{sgn}(\alpha_z) \frac{t_1 L(\mathbf{k})}{|\mathbf{h}(\mathbf{k})|} \sin(\alpha_z) \sin(T|\mathbf{h}(\mathbf{k})|) \right] \\ h'_z(\mathbf{k}) &= \frac{1}{\sin(T\epsilon_z)} \left[ -\text{sgn}(\alpha_z) \sin(\alpha_z) \cos(T|\mathbf{h}(\mathbf{k})|) - \frac{M - 2t_2 \sin(\phi) N(\mathbf{k})}{|\mathbf{h}(\mathbf{k})|} \sin(T|\mathbf{h}(\mathbf{k})|) \cos(\alpha_z) \right] \end{aligned} \quad (4)$$

The energy eigenvalues of  $\mathcal{H}_Z(\mathbf{k})$ , i.e the  $\hat{z}$ -kicked Haldane model, without the offset due to the  $h_0(\mathbf{k})\mathbf{I}$  term of the undriven Haldane model, denoted by  $\epsilon_z$ , is given by

$$\epsilon_z(\mathbf{k}) = \pm \frac{1}{T} \cos^{-1} \left[ \cos(\alpha_z) \cos(T|\mathbf{h}(\mathbf{k})|) - \frac{\text{sgn}(\alpha_z)}{|\mathbf{h}(\mathbf{k})|} (M - 2t_2 \sin(\phi) N(\mathbf{k})) \sin(\alpha_z) \sin(T|\mathbf{h}(\mathbf{k})|) \right] \quad (5)$$

and  $\text{sgn}(\alpha_z)$  in both the equations above is the sign of  $\alpha_z$  function.

This completes a description of the model Hamiltonian we are interested in. We now give a brief overview of the mathematical formalism that shall be used to compute the topological invariant for this model.

### III. COMPUTING THE CHERN INVARIANT AND HALL CONDUCTANCE

The Chern invariant or Chern number for 2-D systems is the topological invariant that captures and quantifies the topological non-trivialities associated with the bands of a periodic system. The general definition involves treating the Bloch functions of the filled bands in any

solid as defining a principal fibre bundle over the FBZ which is a torus. The Chern invariant is then calculated for any given band as the integral of the Berry curvature, which may be obtained from the Berry connection defined on this bundle over the FBZ [1, 98, 99]. This integral may be written in the following manner

$$\mathcal{C} = \int_{\text{BZ}} \mathcal{F}_{k_x, k_y}(\mathbf{k}) dk_x \wedge dk_y \quad (6)$$

where  $\mathcal{F}_{k_x, k_y}$  is an antisymmetric tensor denoting a curvature 2-form, the Berry curvature or field. Haldane's work [94] suggests a simplified route to calculating the Chern number for the various topological phases by an effective linearization of the spectrum at a Dirac point

where the gap is like a mass term and coefficient of the  $\sigma^z$  matrix in the linearized Hamiltonian around this point. The total Chern number for the lower band is then given by the signs of the masses at the two inequivalent Dirac points in the FBZ as

$$\mathcal{C} = \frac{1}{2} \sum_{\nu=\pm 1} \nu \operatorname{sgn}(m_\nu), \quad (7)$$

where  $m_\nu$  is the mass term at the corresponding Dirac point indexed by  $\nu$ . Both the expressions are demonstrably equivalent and one can in principle derive eq.(7) from eq.(6). In our calculations we use both methods to develop the Chern number phase diagram in the presence of driving. The integration is performed numerically to validate the Hall conductivity quantization expected from the second definition.

We intend here to give a brief overview of the mathematical formalism adopted by us to compute the Berry curvature required in the above integral. This formalism is based on the concept of Bargmann invariants [100–102]. It essentially involves the use of  $U(1)$  invariant pure state density matrices  $\rho = |\psi\rangle\langle\psi|$  denote physical states or rays in a complex projective ray space. Then, the Bargmann invariants, are products of these density matrices,  $\rho_1\rho_2\cdots\rho_j$  with the  $j$  states forming the vertices of a  $j$ -sided polygon in ray space. In more explicit terms a Bargmann invariant of order  $j$  for a set of as many normalized states  $|\psi_j\rangle$  such that  $\langle\psi_j|\psi_{j+1}\rangle \neq 0$ , is

$$\mathcal{B}^j(\psi_1, \dots, \psi_j) = \langle\psi_1|\psi_2\rangle\langle\psi_2|\psi_3\rangle\cdots\langle\psi_{j-1}|\psi_j\rangle\langle\psi_j|\psi_1\rangle \quad (8)$$

The phase of the Bargmann invariant in Eq.(8) is obtained as,

$$\mathcal{F}_{\alpha\beta}(\mathbf{x}) = \frac{1}{2i} \operatorname{Tr}(\rho(\mathbf{x})[\partial_\alpha\rho(\mathbf{x}), \partial_\beta\rho(\mathbf{x})]) \quad (9)$$

i.e. the Berry curvature. The  $\mathbf{x} = (x_1, x_2, \dots, x_{2N-2})$  denotes coordinates of points in ray space under some suitable parametrization, ray space being  $(2N-2)$  dimensional for an  $N$ -level quantum system. In the case of lattice systems and Bloch functions these coordinates are  $\mathbf{k}$ -space coordinates  $(k_x, k_y, \dots)$ . The indices  $\alpha$  and  $\beta$  run over the ray space dimensions. It is interesting to note that one can recover the customary expression for the Berry curvature, over the Brillouin zone, for  $2 \times 2$  systems with translational invariance of the kind  $H(\mathbf{k}) = \boldsymbol{\sigma} \cdot \hat{n}(\mathbf{k})$ , which is in general given by

$$\boldsymbol{\Omega}(\mathbf{k}) = \frac{1}{2|\hat{n}(\mathbf{k})|^3} \hat{n}(\mathbf{k}) \cdot [\partial_{k_x} \hat{n}(\mathbf{k}) \times \partial_{k_y} \hat{n}(\mathbf{k})]$$

upon making the substitution  $\rho(\mathbf{k}) = \frac{1}{2}(1 + \boldsymbol{\sigma} \cdot \hat{n}(\mathbf{k}))$  in Eq.(9),  $\mathbf{k}$  serving the role of  $\mathbf{x}$ . This is drawn from a general analogy to the spin- $\frac{1}{2}$  Bloch sphere construction for 2-level systems with Dirac structure. We use Eq.(9) with the same analogy for our  $\hat{z}$ -kicked Haldane Hamiltonian  $\mathcal{H}_Z(\mathbf{k})$ .

The use of density matrices to compute Berry's phase and hence topological invariants has been extended to finite temperature systems with the introduction of Uhlmann's phase [103, 104]. In this case, going beyond pure state density matrices, the use of mixed-state density matrices allows one to go to finite temperature topological phases and characterize them. At low temperatures the invariant from Uhlmann's phase converges to the Chern number. This invariant has even been used to compute the topological phase diagram for the Haldane model at finite temperatures [105]. As a separate study, that we would like to consider in the future, it would be interesting to look at the kicked Haldane model at finite temperatures where topologically non-trivial phases might exist and observe the interplay of kicking and temperature.

## IV. RESULTS AND DISCUSSION

We shall now take up the discussion on (1) the range of driving parameters and their effects on the band structure, (2) effects of periodic kicking on the topological properties of the Haldane model and (3) the modification to Haldane's overlap criterion due to kicking.

### A. Range of Driving Parameters and Effects on Band structure

The Floquet Hamiltonian we have calculated is obtained stroboscopically in an exact manner. Hence, there is in principle no restriction on the chosen driving frequency. However, there are still bounds as to how low one can go. The behavior of the band structure of the driven model requires this lower limit to be set by the convergence of the spectrum of the driven model to the undriven Haldane spectrum in the limit of  $\alpha_z \rightarrow 0$  (i.e. taking the driving to zero). We observe that one can go to a driving frequency of the order of energy  $\approx t_1$ , if the undriven Haldane model, has parameter values  $t_2 = 1$  and  $t_1 = 3$ . This choice of parameters satisfies the overlap prevention requirement.

To put this lower limit in perspective we note when  $M = 0$  and  $t_2 \sin(\phi) = 0$ , the bandwidth of the Haldane model is  $\approx 6t_1$  and hence one can work with a frequency up to this order. In this situation neither inversion nor time-reversal are violated and the system allows bands to touch at both Dirac points in the FBZ. The presence of  $M$  alters the bandwidth but is of no substantial influence if considered smaller than the nearest neighbor hoppings  $t_1$ .

For larger  $M > 3.5$ , there are overlaps of the ground state Floquet bands with the Floquet sidebands for driving period  $\approx 1/t_1$ . In this case it is observed that an upper limit to the driving period  $T = 1/2t_1$  resolves this issue for all  $M$  choices. The issue with larger  $M$  s in the  $1/t_1$  limit case can be resolved at non-zero driving ampli-

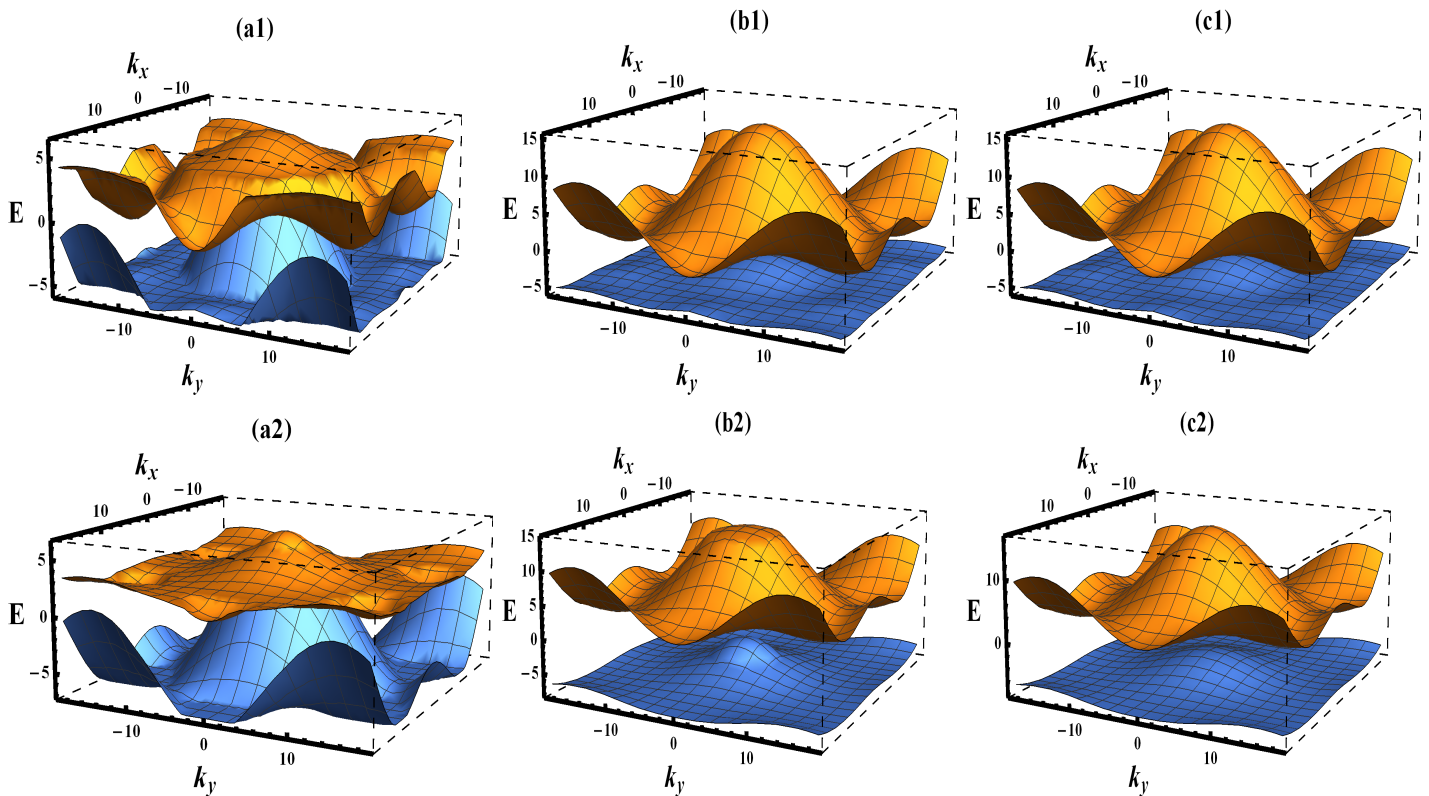


FIG. 2. (Color online) The ground state Floquet bands for the driven Haldane model as seen for different driving frequencies. We consider a driving period of the form  $T = 1/vt_1$  where  $v = 0.5, 1$  and  $2$ . The fixed parameters for all plots are  $\phi = 0$ ,  $t_1 = 3, t_2 = 1$  and  $\alpha_z \approx 0$ . Plots (a1) and (a2) are for  $v = 0.5$  and  $M = 2$  and  $4$  respectively. In these we note that, for zero driving amplitude, the band structure is very much different from that of the undriven case. At this low frequency the distortions are due to overlaps with Floquet sidebands. Plots (b1) and (b2) are for  $v = 1$  and  $M$  values  $2$  and  $5$  respectively. Here, the choice of frequency works for the lower  $M$  value without any higher band interference but for the larger  $M$ , sideband overlaps occur. This is seen from the near flat truncation of the conduction band peak and the bump at the center of the valence band in plot (b2). Plots (c1) and (c2) are for  $v = 2$  and  $M$  values  $2$  and  $5$  respectively. They clearly indicate that this choice of frequency preserves the features of the Haldane spectrum when the driving is taken to zero.

tudes which remove the overlap to the sidebands but this does not hold true when one goes all the way down to zero driving amplitude. Thereby by making  $1/2t_1$  the more favourable choice of upper limit for the period. These features are illustrated in Fig.2.

So, in a driving scheme based on periodic kicking we are able to free the analysis of the constraint of limiting the driving to high frequencies and instead go to comparatively lower values. This feature is absent in the schemes involving continuous drives, such as circularly polarized light, that require the photons of the driving radiation to be of energies larger than the bandwidth [55].

This brings us to the question of how the amplitude of driving influences the features of the driven system. We restrict ourselves to a discussion of how the driving amplitude affects the band structure for a fixed choice of the hopping energies and at some particular choice of  $M$  and  $\phi$ . The driving accentuates the inversion symmetry-breaking and the gap that opens in the spectrum increases as the amplitude is increased. There are however effects on the band curvature. It is known that when the

kicking is applied to graphene, it leads to flat band structures at driving amplitudes of the magnitude  $\alpha_z = \pi/2$  [84]. In the Haldane model one of the crucial differences in the band structure from that of ordinary graphene is the absence of particle hole symmetry (due to the next nearest neighbor hoppings governed by  $t_2$ ). This feature is loosely understood in terms of the greater number of  $B$  sites than  $A$  sites in any finite bounded version of the system.

Thus, for this model, when the amplitude of kicking is similarly increased, the band structure does not become completely flat, especially for the valence band. The conduction band does show nearly perfect flatness when the hopping energies are in the ratio satisfying  $|t_2/t_1| < 1/3$ .

The choice of  $\phi$  here is kept fixed at  $0$  and  $M$  could be non-zero but within the range that shows topological behavior in the undriven case, i.e.  $[-3\sqrt{3}, 3\sqrt{3}]$ . Though one may be cautioned that even in going upto this magnitude of driving the undriven overlap condition begins to break down in favor of a newer one hinted at earlier, but the signatures of flatness can be observed to occur

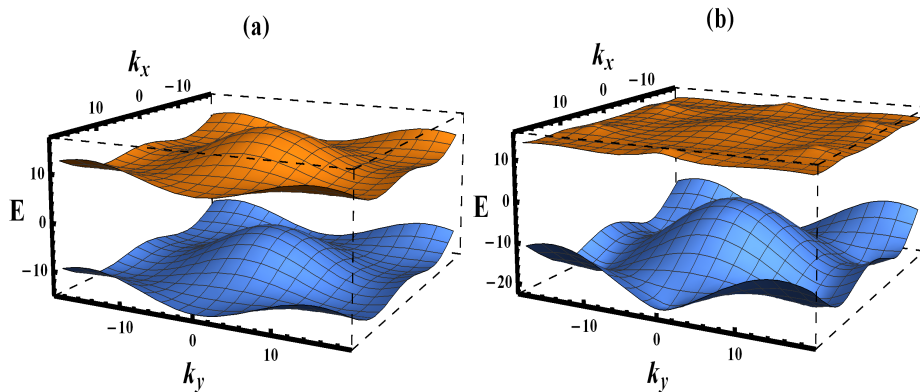


FIG. 3. (Color online) The behavior of the Floquet spectrum at relatively large driving amplitudes for the fixed parameters  $\phi = 0$ ,  $t_1 = 3$  and  $t_2 = 1$ . Plot (a) is for  $\alpha_z = \pi/2$  and  $M = 2$ . It shows the appearance of the tendency to flatness in the band structure especially in the conduction band. Changing the  $M$  value does affect this behavior but the flatness can be found to occur at a suitable corresponding  $\alpha_z$  value. Plot (b) is for  $\alpha_z = \pi$  and  $M = 0$ . We see that the conduction and valence bands have completely exchanged their structures from the undriven case. Important to note that the conduction band now shows almost complete flatness with slight bumps at the Dirac point locations which touch with the minima of the valence band when one accounts for the folding of the Floquet quasienergies. Topologically this has the effect of exactly exchanging the Chern numbers for the bands from the undriven case. This is discussed in detail in Sec.IV B.

well before this threshold is reached. In going beyond the  $\alpha_z = \pm\pi/2$  limit the band structure is found to invert its curvature and as one proceeds to increase the driving to  $\alpha_z = \pi$  the conduction and valence exchange their structure from what is seen near zero driving. The interplay of the magnitude of  $M$  and  $\alpha_z$  is found to effect the degree of flatness of the bands, especially the conduction band. These features are illustrated in Fig.3. We will see that due to the periodicity in the mass term stemming from the nature of the kicking, changing the magnitude of the driving causes the system to undergo a transition in and out of topological phases in a periodic manner. In order to observe the full array of non-trivial topological behavior it suffices to work in the driving amplitude range of  $\alpha_z \in [-(2n+1)\pi/2, (2n+1)\pi/2]$  and further within this range, the original condition to avoid overlap of bands when touchings occur i.e.  $|t_2/t_1| < 1/3$  is valid almost within  $\alpha_z \in [-1, 1]$ . This range is sufficient to observe the competition between  $M$  and the driving in terms of influencing the topological phase, for a fixed choice of hoppings satisfying the above criterion.

However, to maintain sufficient generality in our discussion we will look at topological behavior at large driving amplitudes and the new overlap condition that comes into play in these regimes. A point to note here is that though we fix hopping values while discussing the topological properties at large drivings (thereby falling out of the criterion to avoid overlap of bands at these large driving amplitudes), this effect may be ignored so far as understanding of the topological phases is concerned. If one

is indeed interested in a realization of the driven model at high amplitude kicking and in observing the band touchings in the spectra, an adjustment in the choice of hoppings, especially  $t_2$ , is necessary. Speaking in these terms necessarily assumes that one is working with a system where such parameters as the hopping energies and the site energies are free to be controlled and varied. This seems possible only in optical lattice setups where lattice depths and occupation densities of the ultracold atoms can be manipulated.

## B. Topological features of the kicked model

### 1. Analytical Deductions

We now come to a discussion of the topological properties of the driven Haldane model. Here, we analyze the effects of periodic kicking on the topological phase diagram for the Hamiltonian in eq.(1) [94]. We look at the mass term of our driven model, which is the coefficient of the  $\sigma^z$  matrix in 2D systems, for the various topological phases the system could exhibit. Thus we make use of the definition for obtaining the Chern number  $\mathcal{C}$  given in eq.(7). To apply this we consider  $\epsilon_z(\mathbf{k})h'_z(\mathbf{k})$  from eq.(4), which is the coefficient of  $\sigma^z$  in the driven Haldane Hamiltonian. The technique requires one to consider the gap at the Dirac points  $\mathbf{K}$  and  $\mathbf{K}'$ , and look at the sign of  $h'_z(\mathbf{k})$  in the vicinity of these points. On doing so  $\mathcal{C}$  is given by the expression

$$\mathcal{C} = \frac{1}{2} \sum_{\nu=\pm 1} \nu \text{sgn} \left[ \frac{\epsilon_z(\mathbf{k})}{\sin(\gamma_\nu)} \left( -\text{sgn}(\alpha_z) \sin \alpha_z \cos(T|M - 3\sqrt{3}\nu t_2 \sin \phi) - \text{sgn}(M - 3\sqrt{3}\nu t_2 \sin \phi) \sin(T|M - 3\sqrt{3}\nu t_2 \sin \phi) \cos \alpha_z \right) \right] \quad (10)$$

where,

$$\gamma_\nu = \cos^{-1} \left[ \cos \alpha_z \cos(T|M - 3\sqrt{3}\nu t_2 \sin \phi) - \text{sgn}(\alpha_z) \text{sgn}(M - 3\sqrt{3}\nu t_2 \sin \phi) \sin \alpha_z \sin(T|M - 3\sqrt{3}\nu t_2 \sin \phi) \right] \quad (11)$$

The denominator in the above expression for  $\mathcal{C}$  goes to zero for certain values of the driving  $(\alpha_z, T)$  and the Haldane model parameters  $(M, \phi, t_1, t_2)$ . Out of these the hopping parameters will usually be considered to be fixed for a given realization of the model. Here, we are interested in the general conditions that can be deduced from the form of the Chern number and the behavior of the mass term at the Dirac points under various choices of the driving and model parameters.

Thus the condition for the denominator to go to zero, the mass terms to vanish, and hence Berry curvature to diverge at either of the Dirac points, is given by  $\gamma_\nu = n\pi$ , with  $n = 0, \pm 1, 2, 3, \dots$ . This essentially reduces to the condition  $\cos(|\alpha_z| + T(M - 3\sqrt{3}\nu t_2 \sin \phi)) = \pm 1$  which implies  $|\alpha_z| + T(M - 3\sqrt{3}\nu t_2 \sin \phi) = n\pi$ . The numerator of the expression for  $\mathcal{C}$  (see eq.(10)), apart from the  $\epsilon_z(\mathbf{k})$  term which does not play a role in determining the sign of the term (at the locations for the two Dirac points once one has chosen the valence band for calculating  $\mathcal{C}$ ), go to zero for  $\sin(|\alpha_z| + T(M - 3\sqrt{3}\nu t_2 \sin \phi)) = 0$ . The appearance of the indeterminate  $0/0$  form which seems to occur is regulated in a limiting manner, by the presence of the  $\epsilon_z(\mathbf{k})$  in the numerator. Thus what we have obtained is the condition for the bands to touch at either one of the Dirac points depending on the value of  $\nu$  ( $\pm 1$ ) in the equation  $|\alpha_z| + T(M - 3\sqrt{3}\nu t_2 \sin \phi) = n\pi$ .

This is the modified condition for the boundary sinusoids which enclose the topologically non-trivial phases in the case of the Haldane model under kicking.

A couple of features become apparent from this condition. We observe, that the periodic kicking has the effect of modifying the inversion breaking parameter  $M$  to  $M - \frac{(n\pi - |\alpha_z|)}{T}$  which depends on the driving parameters  $\alpha_z$  and  $T$ . Thus for different values of  $n$ , there is a specific set of values for  $(M, \alpha_z, T)$  which would satisfy phase boundary conditions similar to the conditions satisfied by the Chern number in the Haldane model. In this case we have a periodic recurrence of the phase diagram plotted between  $M/t_2$  and  $\phi$  along the  $M/t_2$  axis, as manifested in repeated copies of the original Chern diagram for the undriven model on moving along this axis. Thus, the broad topological behavior of the undriven model is preserved in the driven model but now extends to newer regions of  $M$  values for a fixed choice of  $t_2$ . The system

under driving begins to explore a larger space of parameters in terms of the occurrence of topological phases. Another feature that comes across is that the new condition for the phase boundaries depends on the magnitude of the driving  $|\alpha_z|$  and is independent of its sign. In fact, the modification to the inversion breaking factor is such that it depends on the ratio  $\alpha_z/T$  which encapsulates the complete effect of the driving. The appearance of the ratio indicates that the amplitude of the driving can be made to scale with the frequency in a linear fashion to obtain a class of driven models with identical topological behavior. There is even the possibility of choosing the amplitude of the kicking to gradually increase, in a linear fashion with time, on a scale adiabatic in comparison to the driving, so as to be effectively regarded as constant over several driving periods. With this one may realize a linear-in-time variation of the inversion breaking term and hence travel from a topologically non-trivial to a topologically trivial phase. This could be of use in schemes looking to quench Chern insulators across a topological phase boundary with a normal insulator to study various properties of dynamical topological phase transitions at the quantum critical point[106].

The effect of increasing the driving amplitude from zero (in either positive or negative sense), i.e. the undriven situation, is to shift the Haldane Chern number phases (pair of lobes due to the intersecting sinusoidal phase boundaries) vertically downwards, from their undriven position, along the  $M/t_2$  axis. This effect applies to all the periodic copies of the phase diagram along this axis. Let  $M'$  be used to denote the new effective inversion breaking parameter in the presence of driving. Thus what we are effectively witnessing is a renormalization of the ‘Semenoff mass’ component  $M$  in the Haldane mass. In the undriven case there was a unique inversion breaking site energy  $M$  with the phase diagram center at  $(M = 0, \phi = 0)$ . This then had corresponded to a graphene like semi-metallic band structure with touchings at both Dirac points. In the driven model this admits multiple values as seen from  $M' \equiv M - \frac{(n\pi - |\alpha_z|)}{T}$  and hence multiple semi-metallic centres  $M - \frac{(n\pi - |\alpha_z|)}{T} = 0, \phi = 0$ . for the different  $n$  and  $\alpha_z$  values. The  $n$  values define a set of several ‘Semenoff Masses’ at a give non-zero kicking all of which are valid choices around which topological phases

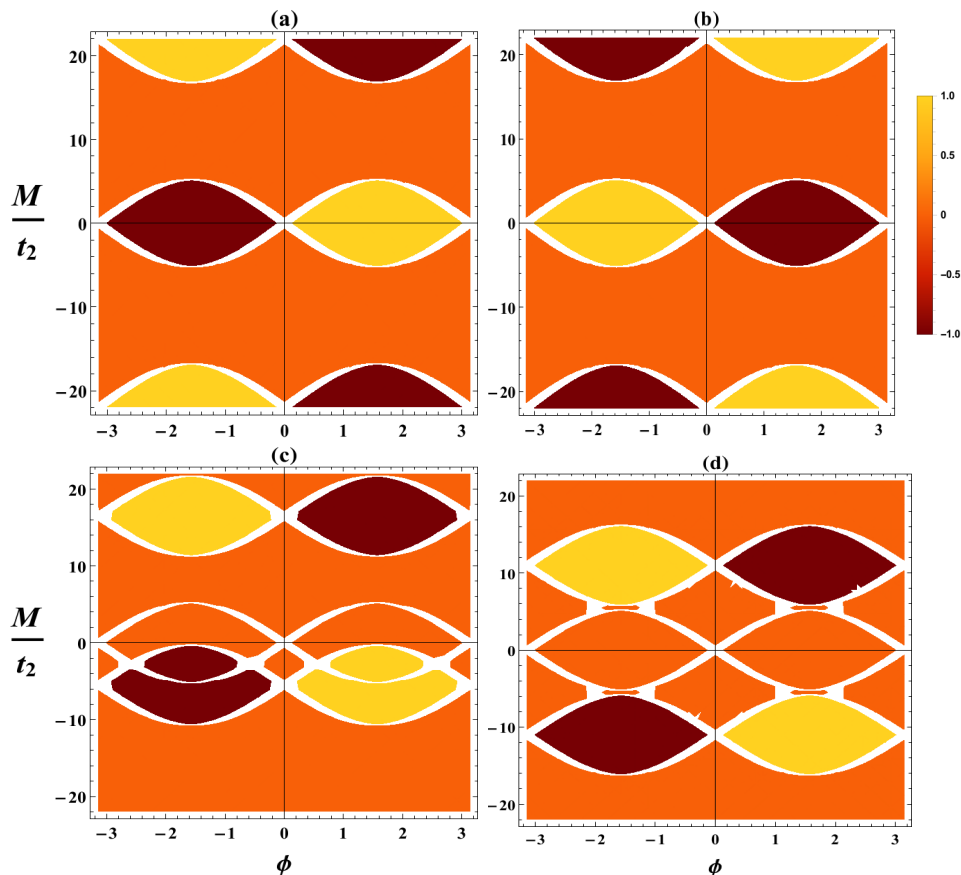


FIG. 4. (Color online) Plots of the Chern number in the  $M/t_2$  and  $\phi$  plane for different  $\alpha_z$  values. The plots (a),(b),(c) and (d) are for  $\alpha_z$  values 0 (**in the limit of weak driving**),  $\pi$ ,  $\pi/4$  and  $\pi/2$  respectively. The darkest regions indicate a Chern number of  $-1$ , the lightest ones  $1$  and the intermediate shade is for  $0$  Chern numbers. The choice of undriven Haldane model hoppings, for these plots, is fixed at  $t_1 = 3.5$  and  $t_2 = 1$ . The driving period is taken to be  $T = \frac{1}{2t_1}$ .

can manifest. There is now a multiplicity of possible undriven Semenoff mass choices  $M$  which yield  $M' = 0$ . The period of driving  $T$ , which we fix with a specific  $t_1$ , decides the separation between the centres for a given driving. Thus the zero driving case does not collapse to a single  $M$  value topological phase structure (the original Haldane model) but still shows a multitude of such phase diagrams which may be regarded as a consequence of the folding or periodicity in Floquet quasienergies. This hints that the topological phase diagrams repeat identically at a separation of  $2\pi/T$  in the  $M$  values which is exactly the width of a quasienergy Brillouin zone.

Varying the driving  $\alpha_z$  on the other hand, for a fixed choice of  $n$  and  $M$ , is a more physically plausible and interesting as that would take a chosen undriven model  $(M, \phi)$  through a topological transition. This is very much like quantum Hall plateau transitions with adiabatically varying magnetic field. An interesting feature that shows up is that for a given kicking amplitude at  $M$  values  $\frac{(n\pi - |\alpha_z|)}{T}$ , for different  $n$  say,  $0$  and  $1$  the Chern number phases are reflected about the  $\phi = 0$  line in the phase diagram. This is of more significance when one varies the driving amplitude  $\alpha_z$  to the relatively high regime of  $\pi$

or  $-\pi$ . Then the Semenoff mass  $M'$  post driving is equal to the undriven one  $M$  for  $n = 1$  which is clear from the relation. So the Chern number phase diagram with its phases reflected about  $\phi = 0$  now occupies the region of the phase diagram where earlier the undriven Haldane Chern number diagram was valid and thus in this extreme driving condition the topological phases undergo an exact inversion. This indicated that even an inversion breaking taken to a certain extreme may alter the band topology of a Chern insulator at least in the presence of driving. However, physically there are issues with such large kicking amplitudes some of which have been discussed earlier.

Again one has to exercise some caution here, on account of the folding of the quasienergies. There is always the possibility of band touchings which occur at the extreme ends of the spectrum (quasienergy Brillouin zone boundaries), besides the conventional ones at the middle of the spectrum which occur in the undriven and driven cases. This could cause the Chern numbers to invert for the two bands. Indeed, what we see here is that, the inversion in phases is due to these band touchings at the  $\pm\pi/T$  limits of the folded spectrum and hence the gap

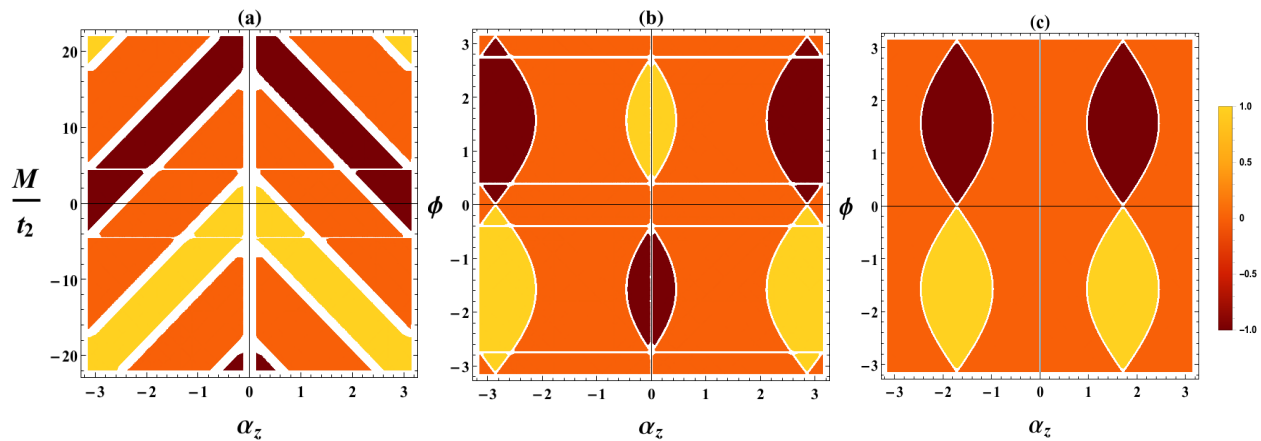


FIG. 5. (Color online) Various sectional views that indicate how the topological phase diagram varies with change in driving amplitude keeping one symmetry breaking parameter fixed and varying the other. Plot (a) indicates such variation for a fixed  $\phi = \pi/3$  and illustrates the linear variation of the phases for different  $M/t_2$  as  $\alpha_z$  is changed. One notes the sharp turn the phases take at  $\alpha_z \rightarrow 0$ , a clear consequence of the dependence of the phases on the driving magnitude  $|\alpha_z|$ . Plots (b) and (c) illustrate phase regions for varying  $\phi$  and  $\alpha_z$ , with  $M/t_2$  choices fixed at 2 and 10 respectively. The Chern number convention for the shaded regions is the same as that for Fig.4.

closing at the edges of the quasienergy Brillouin zone. These arguments sit well with the previous discussion of the appearance of flat band behavior in the conduction band as driving amplitude is increased. As it starts to acquire the curvature characteristics which are present in the valence band in case of zero driving. Thereby an exact reversal of structure occurs between the valence and conduction bands and the Chern numbers flip due to this new closing opening transition. The band structure is shown in Fig. 3(b).

## 2. Evidence from Phase Diagrams

To illustrate the various aspects of the topological phase diagram for the driven Haldane model we refer Fig.(4). These figures are for parameter values  $t_1 = 3.5$  and  $t_2 = 1$  that satisfy the band overlap prevention condition. Again, we caution that variation to this condition in the presence of driving which has been hinted on several earlier occasions and so  $t_2$  has to be changed beyond a certain driving amplitude regime but here this is ignored as the broad topological behavior is unaffected by this. The driving period is fixed at  $T = \frac{1}{2t_1}$ . This choice, as stated earlier, ensures that the limits of the Floquet quasienergy Brillouin zone remain beyond the bandwidth of the undriven model and thus manifests in the phase diagrams as avoided overlaps between the different replicas of the intersecting sinusoids that are seen one below the other in Fig.(4). Other previously discussed features that become apparent include, for instance, one can look at the the plots in Fig.(4) (a) and (b) which are for  $\alpha_z = 0$  and  $\alpha_z = \pi$  respectively and note that when the driving is taken to such extremes the band topology inversion spoken of earlier occurs. Additionally, though  $\alpha_z$  is taken

to tend to zero for the plot (a) and one does indeed see the undriven Haldane model phase diagram around the ( $M = 0, \phi = 0$ ) centre, there are still copies of similar non-trivial topological phases along the  $M/t_2$  axis which are absent in the original Haldane model. This indicates that the stroboscopic Floquet Hamiltonian does not converge to the unperturbed Hamiltonian simply by taking the driving amplitude to zero. This follows from the nature of the identity used to derive the Floquet Hamiltonian (see appendix). Here, the unkicked case can not be obtained from the case with kicking in the straightforward limit of driving amplitude going to zero as the identity breaks down in this case. At best a weak driving limit may be assumed (which is what the plot indicates) that is physically meaningful. It can be seen that substituting  $\alpha_z = 0$  after evaluating the identity one can not get rid of the periodicity in the phase diagram. Thus the weak driving case essentially is a means of, at best, recovering the undriven Haldane model characteristics in the presence of kicking. The periodicity will be non-existent in the case where there is no kicking but this cannot be approached continuously from the Floquet Hamiltonian which, in turn, is not to be regarded as some weak perturbation to the undriven case. One also has to take the limit of the driving period becoming very small and ideally going to zero. It is in this limit that one recovers the undriven model's characteristics and this is true for the phases in plot (a) of fig.(4) as the other topological phase regions will get pushed out to infinity and one obtains Haldane's original phase diagram. An observation that is consistent with the fact that, in the limit of driving frequencies being infinitely large, one is precisely left with the time-averaged Hamiltonian over a period as the exact description of the system. This can be understood in the sense of high frequency expansions for effective Hamiltonians where the zeroth order undriven Hamilto-

nian can only be truly retrieved in the large or infinite frequency limit.

This is so as the separation between two pairs of intersecting sinusoids that delineate two topological phase regions is decided by the corresponding driving renormalized Semenoff masses and the difference between these masses can be seen to depend on the driving frequency. Thus one can easily see that the effect of varying the driving frequency, say decreasing it in our model, would be to bring the adjacent topological regions, enclosed between their respective pair of sinusoids, nearer to one another. Eventually, for the lower driving frequency limit, of which we have spoken earlier, the Haldane-like topological phase diagram copies are close enough for the sinusoids of adjacent diagrams to just touch each other. Going lower in the frequency would take one into the forbidden limit where these non-trivial regions begin to overlap.

Further, if one looks at plots (c) and (d) of fig.(4) we see that for the driving amplitudes of  $\alpha_z = \pi/4$  and  $\pi/2$  respectively one has the effect of shifting the topological phases away from the parameter regions which were topologically non-trivial in the undriven situation. Thus in plot (c) one can clearly see the new topological region shifted with respect to the phase boundary for the undriven model, which is the pair of sinusoids intersecting at the origin in the phase plane. These boundaries are kept specifically to demarcate the topological region of the unkicked Haldane model as reference to emphasize the shifting. Even though, as can be seen in the plots, they enclose topologically trivial regions. In particular the upper half of the region enclosed between the undriven model's phase boundaries is now topologically trivial. Thus, increasing the driving, shifts the phases in a linear fashion. One may consider some choice of undriven model parameters  $M$  and  $\phi$  for which the system is in a topological phase and after a certain magnitude of driving the model enters a topologically trivial phase. Thus the change in the driving amplitude can, as discussed earlier, bring a plateau transition in the Chern number. This effect is more pronounced in plot (d), where, the entire parameter range which was topological in the undriven case is now trivial and hence the driving does offer a path to transition between non-zero and zero Chern numbers and hence may be used to study the normal to Chern insulator transition in such simple non-interacting systems.

Fig.(5) illustrates the topological phases of the kicked model when looked at from different cross-sectional views of the solid three dimensional structure that would result if the various phase plots for the  $\alpha_z$  values, such as those in fig.(4), were stacked in proper sequence, one above the other, along an out of plane  $\alpha_z$  axis. In this figure, all the parameter values that need specification to obtain the plots therein, are chosen to be the same as those used for fig.(4). Plot (a) in the figure depicts the behavior of the topological regions for a  $\phi$  value fixed at  $\pi/3$  and,  $M/t_2$  and  $\alpha_z$  being varied. The linear variation of the phases

in this picture reveals the linear shift in the sinusoidal lobes seen in the plots of fig.(4), with change in driving. Additionally, the sharp turn in slope, as if a reflection, of these linear phase regions, which are basically tubes with sinusoidal cross-sections, at  $\alpha_z = 0$  is indicative of the driving dependence being purely on the magnitude i.e.  $|\alpha_z|$ . Once this picture is established it becomes easier to interpret the other two plots (b) and (c), which show the  $\phi - \alpha_z$  phase plane for  $M/t_2$  values 2 and 10 respectively. Since a constant  $M/t_2$  can be understood as a plane that slices a kind of Pan flute structure of the tubes of intersecting sinusoids. Thus on the plane one expects to get the projections of the tubes that are cut and this naturally depends on where one chooses to slice. So, where such flutes of different inclination meet, which is at the turning point i.e.  $\alpha_z = 0$  or, if one considers the full periodicity,  $n\pi$ , they form an intersecting sinusoidal edge. If the slice is chosen that it cuts above or below the exact centre of this ridge i.e.  $M \neq 0$  then the projection on the corresponding  $\phi - \alpha_z$  plane will have a pair of non-touching sinusoids at the centre. This is what shows up in the middle of plot (b). Of course the slice may be so chosen that it lies outside this intersecting sinusoidal edge in which case it will cut the nearest sloping flute tubes and result in a projection with touching sinusoids, as is the case in plot (c). Due to the inherent periodicity in the phase diagram structure, as one goes through a complete period of the  $M/t_2$  choices, the projections begin to show the underlying periodicity.

Before proceeding further, we would like to compare and contrast our model with other similar studies in the literature [85]. In this work the authors look at the impact that periodic kicking has on the QWZ Chern insulator, a model similar to the Haldane model in that it admits complex valued hoppings, which features in the models for the quantum spin Hall effect. The study shows that for  $\hat{z}$ -kicking the QWZ insulator exhibits topological phases with higher order Chern numbers. The authors attribute this to merging and splitting of Dirac cones and the appearance of long-range hoppings due to driving. Our model, on the other hand, does not exhibit higher order Chern numbers. The criteria for band touchings essentially remains the same both before and after driving at least to the extent that the number of Dirac points within the first Brillouin zone remains unchanged. The Chern numbers associated with the topological phases remain the same after driving. Even if long-range hoppings do appear, the Chern numbers of the  $\hat{z}$ -kicked Haldane model are robust to these, unlike in the QWZ model.

### C. Modifications to Haldane's overlap criterion due to kicking

This broadly concludes our discussion of the topological features of the kicked Haldane model. We now turn our attention to the issue of avoiding band overlap in the presence of driving, a concern which has been repeat-

edly expressed at various points in the above discussion under different contexts. The prime consideration is to have the bands touch in a way that the spectrum allows these touchings to be detected without ambiguity. This imposes a relation on the hopping parameters. As the

relative magnitude of  $t_1$  and  $t_2$  has the effect of influencing the degree of particle-hole symmetry breaking in the system, and hence, the nature of the touchings. Along lines similar to the arguments for Haldane's criterion we obtain the following condition that needs to be satisfied

$$9t_2 < \cos^{-1} \left[ \cos(\alpha_z) \cos \left( T \sqrt{9t_1^2 + M^2} \right) - \frac{M \sin(\alpha_z) \sin(T \sqrt{9t_1^2 + M^2})}{\sqrt{9t_1^2 + M^2}} \right] - \cos^{-1} \left[ \cos(\alpha_z) \cos(T|M|) - \text{sgn}(M) \sin(\alpha_z) \sin(T|M|) \right] \quad (12)$$

In the above inequality, a condition is imposed on the suitable values for  $t_2$  once  $t_1$  has been chosen. This is accompanied with the effects of driving also having a role to play in the determination of this value. Both the driving amplitude  $\alpha_z$  and the driving period  $T$  appear in the above expression. Since we have already done so in our earlier analysis  $T$  can be taken to depend in an appropriate way on the nearest neighbor hoppings  $t_1$ . The  $M$  can be written in terms of the driving amplitude using the previously derived expressions for the new Semenoff masses  $M'$  depending on which  $n$ -th order semi-metallic center one is looking at to observe the band touchings, by putting that particular choice of  $M'$  to zero or  $n\pi$ . Thus the condition can be reduced to depend solely on  $\alpha_z$  and  $t_1$ . Another feature of this condition is that unlike the ordinary one given by Haldane which has a simpler reciprocal relationship between the two hopping energies, the above relation is not easily invertible to a case where one fixes  $t_1$  and calculates the condition on  $t_2$ . In the context of varying  $\alpha_z$  for a fixed  $n$  in the choice of  $M'$  or changing  $n$  for fixed  $\alpha_z$  the variation in the choice of  $t_2$  will have the effect of altering the boundary sinusoids of the corresponding phase diagrams in the parameter space. Thus if one were to rigorously enforce this condition, which we have ignored for now in the phase diagrams in fig.(4) where  $t_2$  is fixed at unity, we would observe a flattening or broadening of the pair of intersecting sinusoids. This follows from the fact that changing  $t_2$  say in the diagram of a given  $\alpha_z$  for different  $M$  and hence  $n$  values would rescale the vertical axis of the diagram. We would like to point out that adjusting  $t_2$  is a freedom available only in certain realizations, as mentioned earlier, hence, if one is interested in driving the system across a topological transition it would be reasonable to do so in the previously suggested range of  $\alpha_z \in [-1, 1]$ . Since within this domain the ordinary haldane condition is a workable choice and one need not be concerned too much about the effects of driving in this regard.

## V. EXPERIMENTAL ASPECTS

We elaborate here, some of the ideas that were mentioned in the introduction relating to the experimental realization of our kicked model. The exact realization of a kicking scheme is an experimentally formidable challenge owing to finite response and relaxation times of physical systems. There are however, a few proposals, that deserve mention as they may simulate a periodic driving which can in a suitable limit yield the effects of kicking. From an actual material realization perspective, the Silicene based Haldane model of [87] can be driven using the schemes cited in [84] to simulate similar kicking but in graphene. In [84] the authors cite a method that involves placing a sample of hexagonal boron nitride over a layer of graphene in such a way that adjacent boron and nitrogen atoms are positioned over neighbouring carbon atoms of graphene [91–93]. Such a structural arrangement is permitted by the almost identical lattice constants of both materials. This proposal of [84] is motivated by its capacity to realize an effective sublattice potential for the underlying graphene layer. Once this configuration is established the driving is implemented by applying periodically varying pressure on the two layers such that the distance between them varies periodically in time. This would effectively vary the sublattice potential experienced by the carbon atoms belonging to the A and B sublattices of graphene and thus produce the effects of z-kicking. This could be replicated in the Silicene based realization by an appropriate choice of a transition metal dichalcogenide that fits the lattice spacing.

The other possible platform for realizing our model is using a cold-atom optical lattice setup. Such a quantum simulation of the Haldane model [30] may be subjected to a pulsing that can be designed to impart the effects of driving using a periodic train of delta-function kicks [107]. The technique in its present form simulates a 2-D rectangular lattice with a synthetic magnetic field by subjecting a gas of ultra-cold alkali metal atoms to a pair of counter-propagating Raman lasers in one direction and a magnetic field gradient perpendicular to this. The Raman lasers are tuned near resonance in such a way as to give a multi-frequency coupling term which, along with

the position dependent detuning gradient, in the time domain gives a  $2 \times 2$  delta-function kicking with a position dependent strength. Though this method cites the lack of an initial confining optical lattice as a convenience since this eliminates any restrictions on the modulation frequency to avoid transitions between the pre-existing Bloch bands, any scheme for realizing our model would possibly require the presence of a hexagonal or brick-like optical lattice [30] on which the kicking is realized. Further the advantages offered with respect to heating effects due to interactions or micromotion could be adversely affected under such modifications.

As regards the possibilities of heating and thermalization in our system, certain remarks are in order. The Haldane model being driven is a free fermion model in the non-interacting, single particle approximation. The overall dynamics of the Floquet system is integrable and hence one in general does not expect heating to infinite temperatures over long times, due to the driving [108]. There is however recent work that suggests the possibility of heating in periodically driven systems that are integrable [109] owing to divergences in the Floquet-Magnus expansion for the effective Hamiltonian at small enough driving frequency. This, however, is not an issue in our closed form stroboscopic Floquet Hamiltonian for the kicked system, where although the component Hamiltonians describing a single period of evolution do not commute with each other the expansion still converges for all frequencies. This follows from the identity discussed in the appendix. What has been said thus far takes the viewpoint of the formalism that is used to describe our system where, in the absence of interactions or disorder, there is little likelihood of many-body localized phases. Though one may reasonably expect to find dynamically localized wavefunctions as was demonstrated in [84]. But from an experimental viewpoint, say in a material realization, these assumptions may not hold and heating could occur. In such situations choosing the driving frequency to be high would help to make the heating rate exponentially slow, as it decays exponentially in the driving frequency. The heating time is therefore large and one should be able to observe the Floquet topological phenomena on experimentally reasonable time scales that are not exponentially large in the frequency. In this case the existence of many-body localized phases is a distinct possibility especially at large frequencies, ensuring the system does not thermalize. Though this might require certain restrictions on system size and hopping/interaction energies when one speaks of finite size systems. Although, in our formalism, we work with the assumption of infinite system size, as can be seen from the hamiltonian for the Haldane model. The authors in [109] suggest heating to infinite temperatures for Floquet systems with integrability as an asymptotic phenomenon in the limit of driving period and system size going to infinity. This too is observed only for choices of random or quasiperiodic fields within a single driving period. For the case of a staggered field the long time

steady state is never found to correspond to an infinite temperature state even for the infinite frequency and size limits. This suggests that even our kicked infinite system should be immune to the possibility of heating to infinite temperature, from a theoretical perspective.

## VI. CONCLUSION

We have considered a  $\hat{z}$ -kicked Haldane model and examine the topological properties of this system. The effects of driving on the topological phase diagram of Haldane's originally proposed model are illustrated. We find that, besides introducing a periodicity in the phase diagram where the Haldane phase diagram is repeated at regular intervals along the inversion breaking axis  $M/t_2$ , a signature of the periodicity of the Floquet quasienergy spectrum, the driving magnitude is solely responsible for a linear shift in the topological phases of the driven model relative to their undriven counterparts. This suggests the use of this driven model to study Floquet topological phase transitions.

This is different from the optically driven Haldane models of [55, 95] where the tunable parameter toys with the time-reversal symmetry breaking by modifying those terms of the effective Hamiltonian which depend on the phase of the complex valued next-nearest neighbor hoppings of the undriven Haldane model. Although the overall effect is to still traverse between topological and non-topological regions of the Haldane Chern number phase plot as drawn against the symmetry breaking parameters, yet this is brought about in a different manner. To be precise this distinction becomes fully apparent when one considers the effective Hamiltonian post-driving in the vicinity of a Dirac point which of course would be usually gapped in the given case. The manner in which the topological phases transition with change in driving amplitude is also different in [55], compared to our case, as there, the sinusoids of the topological phase boundaries undergo a contraction-expansion in a periodic manner instead of the linear shifting that is seen in our case. Also, the driving at sufficiently large amplitudes causes a modification of the band overlap avoidance criterion as originally suggested by Haldane in his model.

Finally, we would like to mention that this kicking scheme could be also applied to the Kane-Mele model for spin orbit coupling in hexagonal lattices [10, 11] to study the effect of driving on the  $Z_2$  topological index which characterizes the topology in such QSHE systems. This is proposed as a future work that we intend to undertake.

## VII. ACKNOWLEDGEMENTS

T.M. thanks UGC, India for funding through a SRF and would like to acknowledge discussions with Prof. Diptiman Sen, Prof. Amit Dutta and Dr. Utso

Bhattacharya in meetings at ICTS. A.P. would like to thank Dr. Adhip Agarwala for valuable inputs. T.G.S and J.N.B thank DST-SERB, India for Project No. EMR/2016/003289. They would also like to thank Prof. T. Oka for discussions and Prof. N. Mukunda for providing his lecture notes on various aspects of geometric phase.

## Appendix

In order to obtain the Floquet Hamiltonian for the kicked system we make use of a well known identity from the algebra of Pauli matrices, which allows one to write

$$e^{ip(\hat{n}\cdot\boldsymbol{\sigma})}e^{iq(\hat{m}\cdot\boldsymbol{\sigma})} = e^{ig(\hat{l}\cdot\boldsymbol{\sigma})}. \quad (\text{A.1})$$

Where,  $p, q$  and  $g$  are scalars and  $\hat{n}, \hat{m}$  and  $\hat{l}$  are unit vectors and for known  $p, q$  and  $\hat{n}, \hat{m}, g$  and  $\hat{l}$  are given by

the relations

$$\begin{aligned} \cos g &= \cos p \cos q - \hat{n} \cdot \hat{m} \sin p \sin q \\ \hat{l} &= \frac{1}{\sin g} (\hat{n} \sin p \sin q + \hat{m} \sin q \cos p \\ &\quad - \hat{n} \times \hat{m} \sin p \sin q) \end{aligned} \quad (\text{A.2})$$

From section II we see that the time evolution over a period is  $U_{XYZ} = U_{kick}U_{static} = e^{-i\boldsymbol{\alpha}\cdot\boldsymbol{\sigma}}e^{-i\mathcal{H}(\mathbf{k})T}$ . We shall use the above identity to compute the Floquet Hamiltonian  $\mathcal{H}_{XYZ}$ , such that  $U_{XYZ} = e^{-i\mathcal{H}_{XYZ}(\mathbf{k})T}$ . To do this we set up the correspondence between the quantities of the evolution operator and the variables in the LHS of eq.(A.1) as,

$$\begin{aligned} p &= -|\boldsymbol{\alpha}| \\ q &= -T|\mathbf{h}(\mathbf{k})| \\ \hat{n} &= \frac{\boldsymbol{\alpha}}{|\boldsymbol{\alpha}|} \\ \hat{m} &= \frac{1}{|\mathbf{h}(\mathbf{k})|} (t_1 L(\mathbf{k}), t_1 F(\mathbf{k}), M - 2t_2 N(\mathbf{k}) \sin \phi) \end{aligned} \quad (\text{A.3})$$

On substituting the above in the relations of eq.(A.2) we can compute the values of  $g$  and  $\hat{l}$  respectively. We are interested in the case of  $\hat{z}$ -kicking and so one needs to additionally impose the conditions  $\alpha_z \neq 0$  while  $\alpha_x = \alpha_y = 0$ . The Floquet Hamiltonian for this case is denoted by  $\mathcal{H}_Z$ . In our case  $g$  corresponds to the Floquet spectrum as  $g = T\epsilon_z(\mathbf{k})$  and the unit vector  $\hat{l}$  to  $\mathbf{h}'(\mathbf{k})$ , as can be seen from section II. Thus we get the vector components  $(h'_x(\mathbf{k}), h'_y(\mathbf{k}), h'_z(\mathbf{k}))$  in eq.(4) and the Floquet band spectrum  $\epsilon_z(\mathbf{k})$  in eq.(5).

- 
- [1] D. J. Thouless, M. Kohmoto, M. P. Nightingale, and M. den Nijs, Phys. Rev. Lett. **49**, 405 (1982).  
[2] B. I. Halperin, Phys. Rev. B **25**, 2185 (1982).  
[3] J. E. Avron, R. Seiler, and B. Simon, Phys. Rev. Lett. **51**, 51 (1983).  
[4] Q. Niu, D. J. Thouless, and Y.-S. Wu, Phys. Rev. B **31**, 3372 (1985).  
[5] Y. Hatsugai, Phys. Rev. Lett. **71**, 3697 (1993).  
[6] K. v. Klitzing, G. Dorda, and M. Pepper, Phys. Rev. Lett. **45**, 494 (1980).  
[7] R. B. Laughlin, Phys. Rev. B **23**, 5632 (1981).  
[8] B. A. Bernevig and S.-C. Zhang, Phys. Rev. Lett. **96**, 106802 (2006).  
[9] B. A. Bernevig, T. L. Hughes, and S.-C. Zhang, Science **314**, 1757 (2006), <http://science.sciencemag.org/content/314/5806/1757.full.pdf>  
[10] C. L. Kane and E. J. Mele, Phys. Rev. Lett. **95**, 226801 (2005).  
[11] C. Kane and E. Mele, Phys. Rev. Lett. **95**, 146802 (2005).  
[12] L. Fu, C. L. Kane, and E. J. Mele, Phys. Rev. Lett. **98**, 106803 (2007).  
[13] J. E. Moore, Nature **464**, 194 (2010).  
[14] Y. Chen, J. Analytis, J.-H. Chu, Z. Liu, S.-K. Mo, X.-L. Qi, H. Zhang, D. Lu, X. Dai, Z. Fang, et al., Science **325**, 178 (2009).  
[15] M. Z. Hasan, S.-Y. Xu, D. Hsieh, L. A. Wray, and Y. Xia, arXiv preprint arXiv:1401.0848 (2014).  
[16] M. Z. Hasan and C. L. Kane, Rev. Mod. Phys. **82**, 3045 (2010).  
[17] X.-L. Qi and S.-C. Zhang, Rev. Mod. Phys. **83**, 1057 (2011).  
[18] A. Altland and M. R. Zirnbauer, Phys. Rev. B **55**, 1142 (1997).  
[19] A. P. Schnyder, S. Ryu, A. Furusaki, and A. W. W. Ludwig, Phys. Rev. B **78**, 195125 (2008).  
[20] A. Kitaev, in AIP Conference Proceedings, Vol. 1134 (2009).  
[21] A. H. Castro Neto, F. Guinea, N. M. R. Peres, K. S. Novoselov, and A. K. Geim, Rev. Mod. Phys. **81**, 109 (2009).  
[22] S. Das Sarma, S. Adam, E. H. Hwang, and E. Rossi, Rev. Mod. Phys. **83**, 407 (2011).  
[23] M. O. Goerbig, Rev. Mod. Phys. **83**, 1193 (2011).  
[24] P. Delplace, D. Ullmo, and G. Montambaux, Phys. Rev. B **84**, 195452 (2011).

- [25] Y. Hatsugai, T. Fukui, and H. Aoki, *Phys. Rev. B* **74**, 205414 (2006).
- [26] Y. Zhang, Y.-W. Tan, H. L. Stormer, and P. Kim, *Nature* **438**, 201 (2005).
- [27] S. Koghee, L.-K. Lim, M. O. Goerbig, and C. M. Smith, *Phys. Rev. A* **85**, 023637 (2012).
- [28] L. Tarruell, D. Greif, T. Uehlinger, G. Jotzu, and T. Esslinger, *Nature* **483**, 302 (2012).
- [29] M. C. Rechtsman, Y. Plotnik, J. M. Zeuner, D. Song, Z. Chen, A. Szameit, and M. Segev, *Phys. Rev. Lett.* **111**, 103901 (2013).
- [30] G. Jotzu, M. Messer, R. Desbuquois, M. Lebrat, T. Uehlinger, D. Greif, and T. Esslinger, *Nature* **515**, 237 (2014).
- [31] T. Oka and H. Aoki, *Phys. Rev. B* **79**, 081406 (2009).
- [32] T. Kitagawa, T. Oka, A. Brataas, L. Fu, and E. Demler, *Phys. Rev. B* **84**, 235108 (2011).
- [33] Z. Gu, H. A. Fertig, D. P. Arovas, and A. Auerbach, *Phys. Rev. Lett.* **107**, 216601 (2011).
- [34] E. Suárez Morell and L. E. F. Foa Torres, *Phys. Rev. B* **86**, 125449 (2012).
- [35] T. Iadecola, D. Campbell, C. Chamon, C.-Y. Hou, R. Jackiw, S.-Y. Pi, and S. V. Kusminskiy, *Phys. Rev. Lett.* **110**, 176603 (2013).
- [36] P. Delplace, A. Gómez-León, and G. Platero, *Phys. Rev. B* **88**, 245422 (2013).
- [37] P. M. Perez-Piskunow, G. Usaj, C. A. Balseiro, and L. E. F. F. Torres, *Phys. Rev. B* **89**, 121401 (2014).
- [38] G. Usaj, P. M. Perez-Piskunow, L. E. F. Foa Torres, and C. A. Balseiro, *Phys. Rev. B* **90**, 115423 (2014).
- [39] P. M. Perez-Piskunow, L. E. F. Foa Torres, and G. Usaj, *Phys. Rev. A* **91**, 043625 (2015).
- [40] M. Sentef, M. Claassen, A. Kemper, B. Moritz, T. Oka, J. Freericks, and T. Devereaux, *Nature communications* **6** (2015).
- [41] J. Cayssol, B. Dóra, F. Simon, and R. Moessner, *physica status solidi (RRL) Rapid Research Letters* **7**, 101 (2013).
- [42] M. Bukov, L. D'Alessio, and A. Polkovnikov, *Advances in Physics* **64**, 139 (2015), arXiv:1407.4803 [cond-mat.quant-gas].
- [43] Y. T. Katan and D. Podolsky, *Phys. Rev. Lett.* **110**, 016802 (2013).
- [44] Y. Wang, H. Steinberg, P. Jarillo-Herrero, and N. Gedik, *Science* **342**, 453 (2013).
- [45] Q.-J. Tong, J.-H. An, J. Gong, H.-G. Luo, and C. H. Oh, *Phys. Rev. B* **87**, 201109 (2013).
- [46] A. G. Grushin, A. Gómez-León, and T. Neupert, *Phys. Rev. Lett.* **112**, 156801 (2014).
- [47] C. He and Z. Zhang, *Physics Letters A* **378**, 3200 (2014).
- [48] L. Zhou, H. Wang, D. Y. Ho, and J. Gong, *The European Physical Journal B* **87**, 204 (2014).
- [49] E. Anisimovas, G. Žlabys, B. M. Anderson, G. Juzeliūnas, and A. Eckardt, *Phys. Rev. B* **91**, 245135 (2015).
- [50] M. Benito and G. Platero, *Physica E: Low-dimensional Systems and Nanostructures* **74**, 608 (2015).
- [51] A. Farrell and T. Pereg-Barnea, *Phys. Rev. B* **93**, 045121 (2016).
- [52] L. Zhou, C. Chen, and J. Gong, *Phys. Rev. B* **94**, 075443 (2016).
- [53] T.-S. Xiong, J. Gong, and J.-H. An, *Phys. Rev. B* **93**, 184306 (2016).
- [54] K. Saha, *Phys. Rev. B* **94**, 081103 (2016).
- [55] J.-i. Inoue and A. Tanaka, *Phys. Rev. Lett.* **105**, 017401 (2010).
- [56] B. Dóra, J. Cayssol, F. Simon, and R. Moessner, *Phys. Rev. Lett.* **108**, 056602 (2012).
- [57] N. H. Lindner, D. L. Bergman, G. Refael, and V. Galitski, *Phys. Rev. B* **87**, 235131 (2013).
- [58] A. Kundu, H. A. Fertig, and B. Seradjeh, *Phys. Rev. Lett.* **113**, 236803 (2014).
- [59] D. Y. H. Ho and J. Gong, *Phys. Rev. Lett.* **109**, 010601 (2012).
- [60] H. Deghani, T. Oka, and A. Mitra, *Phys. Rev. B* **90**, 195429 (2014).
- [61] V. Dal Lago, M. Atala, and L. E. F. Foa Torres, *Phys. Rev. A* **92**, 023624 (2015).
- [62] P. Titum, E. Berg, M. S. Rudner, G. Refael, and N. H. Lindner, *Phys. Rev. X* **6**, 021013 (2016).
- [63] M. C. Rechtsman, J. M. Zeuner, Y. Plotnik, Y. Lumer, D. Podolsky, F. Dreisow, S. Nolte, M. Segev, and A. Szameit, *Nature* **496**, 196 (2013), letter.
- [64] W. Zheng and H. Zhai, *Phys. Rev. A* **89**, 061603 (2014).
- [65] M. D. Reichl and E. J. Mueller, *Phys. Rev. A* **89**, 063628 (2014).
- [66] Z. Yan, B. Li, X. Yang, and S. Wan, *Scientific Reports* **5**, 16197 EP (2015), article.
- [67] A. Verdeny and F. Mintert, *Phys. Rev. A* **92**, 063615 (2015).
- [68] D. Leykam, M. C. Rechtsman, and Y. D. Chong, *Phys. Rev. Lett.* **117**, 013902 (2016).
- [69] M. Račiūnas, G. Žlabys, A. Eckardt, and E. Anisimovas, *Phys. Rev. A* **93**, 043618 (2016).
- [70] T. Kitagawa, E. Berg, M. Rudner, and E. Demler, *Phys. Rev. B* **82**, 235114 (2010).
- [71] A. Gómez-León and G. Platero, *Phys. Rev. Lett.* **110**, 200403 (2013).
- [72] M. S. Rudner, N. H. Lindner, E. Berg, and M. Levin, *Phys. Rev. X* **3**, 031005 (2013).
- [73] D. Carpentier, P. Delplace, M. Fruchart, and K. Gawędzki, *Phys. Rev. Lett.* **114**, 106806 (2015).
- [74] F. Nathan and M. S. Rudner, *New Journal of Physics* **17**, 125014 (2015).
- [75] I. C. Fulga and M. Maksymenko, *Phys. Rev. B* **93**, 075405 (2016).
- [76] M. Fruchart, *Phys. Rev. B* **93**, 115429 (2016).
- [77] R. Roy and F. Harper, *ArXiv e-prints* (2016), arXiv:1603.06944 [cond-mat.str-el].
- [78] R. W. Bomantara, G. N. Raghava, L. Zhou, and J. Gong, *Phys. Rev. E* **93**, 022209 (2016).
- [79] M. Lababidi, I. I. Satija, and E. Zhao, *Phys. Rev. Lett.* **112**, 026805 (2014).
- [80] H. Wang, D. Y. H. Ho, W. Lawton, J. Wang, and J. Gong, *Phys. Rev. E* **88**, 052920 (2013).
- [81] M. Thakurathi, A. A. Patel, D. Sen, and A. Dutta, *Phys. Rev. B* **88**, 155133 (2013).
- [82] D. Babajanov, D. U. Matrasulov, and R. Egger, *The European Physical Journal B* **87**, 258 (2014).
- [83] U. Bhattacharya, S. Dasgupta, and A. Dutta, *The European Physical Journal B* **89**, 216 (2016).
- [84] A. Agarwala, U. Bhattacharya, A. Dutta, and D. Sen, *Phys. Rev. B* **93**, 174301 (2016).
- [85] L. C. Wang, X. P. Li, and C. F. Li, *Phys. Rev. B* **95**, 104308 (2017).
- [86] K. Plekhanov, G. Roux, and K. Le Hur, *Phys. Rev. B* **95**, 045102 (2017).

- [87] A. R. Wright, **3**, 2736 EP (2013), article.
- [88] A. M. Cook and A. Paramekanti, Phys. Rev. Lett. **113**, 077203 (2014).
- [89] A. M. Cook, Phys. Rev. B **94**, 205135 (2016).
- [90] T. Li and O. P. Sushkov, Phys. Rev. B **94**, 155311 (2016).
- [91] J. Jung, A. M. DaSilva, A. H. MacDonald, and S. Adam, Nature Communications **6**, 6308 EP (2015), article.
- [92] C. Ortix, L. Yang, and J. van den Brink, Phys. Rev. B **86**, 081405 (2012).
- [93] M. Weinberg, C. Staarmann, C. Ischlger, J. Simonet, and K. Sengstock, 2D Materials **3**, 024005 (2016).
- [94] F. D. M. Haldane, Phys. Rev. Lett. **61**, 2015 (1988).
- [95] Y.-X. Wang, F.-X. Li, and Y.-M. Wu, EPL (Europhysics Letters) **99**, 47007 (2012).
- [96] T. Thonhauser and D. Vanderbilt, Phys. Rev. B **74**, 235111 (2006).
- [97] A. A. Soluyanov and D. Vanderbilt, Phys. Rev. B **83**, 035108 (2011).
- [98] M. V. Berry, Proceedings of the Royal Society of London A: Mathematical, Physical and Engineering Sciences **392**, 45 (1984), <http://rspa.royalsocietypublishing.org/content/392/1802/45.full.pdf>.
- [99] M. Kohmoto, Annals of Physics **160**, 343 (1985).
- [100] N. Mukunda and R. Simon, Annals of Physics **228**, 205 (1993).
- [101] N. Mukunda and R. Simon, Annals of Physics **228**, 269 (1993).
- [102] E. M. Rabei, Arvind, N. Mukunda, and R. Simon, Phys. Rev. A **60**, 3397 (1999).
- [103] O. Viyuela, A. Rivas, and M. A. Martin-Delgado, Phys. Rev. Lett. **112**, 130401 (2014).
- [104] O. Viyuela, A. Rivas, and M. A. Martin-Delgado, Phys. Rev. Lett. **113**, 076408 (2014).
- [105] Z. Huang and D. P. Arovas, Phys. Rev. Lett. **113**, 076407 (2014).
- [106] U. Bhattacharya and A. Dutta, Phys. Rev. B **95**, 184307 (2017).
- [107] T. Andrijauskas, I. B. Spielman, and G. Juzeliunas, ArXiv e-prints (2017), arXiv:1705.11101 [cond-mat.quant-gas].
- [108] V. Gritsev and A. Polkovnikov, SciPost Phys. **2**, 021 (2017).
- [109] T. Ishii, T. Kuwahara, T. Mori, and N. Hatano, ArXiv e-prints (2017), arXiv:1712.03367 [cond-mat.stat-mech].